Geophys. J. Int. (2002) **150,** 573–587

Correlation between sea surface topography and bathymetry in shallow shelf waters in the Western Mediterranean

G. Rodríguez Velasco and M. J. Sevilla

Instituto de Astronomía y Geodesia (UCM-CSIC), Universidad Complutense, 28040 *Madrid, Spain*

Accepted 2002 January 9. Received 2001 November 26; in original form 2000 September 26

SUMMARY

In this paper, gravimetric and altimetric data are used to assess an estimation of the sea surface topography in the Western Mediterranean Sea. This is a complex area from different points of view, due to the presence of several islands, coastal lines, shallow waters and a peculiar hydrologic equilibrium due to its proximity to the Atlantic water exchange area.

First, a gravimetric geoid was computed using the least-squares collocation (LSC) procedure with the classical remove-restore technique. We also present a local mean sea surface generated from repeat ERS-1 altimeter data fitted to TOPEX. We chose this satellite because it offers a better spatial resolution than the TOPEX data. The time span used in the computations is one year. This is a useful interval for averaging out the regular seasonal variations, which are very large in this area.

We present the comparisons between the gravimetric geoidal heights and the adjusted sea surface. This is a way to obtain a rough estimation of the sea surface topography (SST) since we also include the errors in the two surfaces and other oceanic signals. The differences obtained are physically reasonable with a mean of 17 cm and standard deviation (s.d.) of 39 cm.

A significant similarity is observed between the features reproduced by these differences and the bathymetry in the area, suggesting some sort of correlation between both magnitudes for the studied region. If we accept such correlation, the SST may be described as a function of depth. This procedure lets us filter out the short wavelength part of the geoid from the first SST estimation.

Key words: geoid, LSC, satellite geodesy, sea surface topography.

1 INTRODUCTION

Satellite altimeter data pose several problems in areas close to coastal lines and in shallow waters. First, they can be less accurate due to uncertainties in the applied corrections, especially inaccurate tide estimations. Even if we have accurate corrected data, several obstacles remain. Basins such as the test area are subject to large seasonal changes, which must be removed or else the results may contain major biases. In such an event, the period of time taken into account in the computations becomes a very important factor to consider. Moreover, these basins are usually small and the islands and irregular coastline shapes may cause data interruptions. Then we need to analyse what type of process should be used to remove the radial orbit error, among other items. For instance, crossover adjustment might be unsuitable because the rank deficiency is unknown in these cases.

Following some appropriate treatment, the corrected measurements can provide the mean sea surface, h_{mean}, after removing the uncorrected orbit errors and the seasonal variations. This surface mostly reflects the marine geoid, N. However, due to the ocean dynamics and other circumstances, this result is not an equipotential surface of the gravity field, so it still is not the geoid. The differences between them or mean sea surface height above the geoid, establish what we call the sea surface topography, SST or ς. The SST is composed of a constant or almost stationary part, ς_{o}, which represent the widely main part of the SST, and a variable part, ς_{r}, or mean sea surface variability, much smaller than the first (Heck & Rummel 1989; Rummel 1993; Visser *et al.* 1993; Wang & Rapp 1994; Hipkin 2000) (see Fig. 1). Therefore, if we wish to determine the geoid from altimeter data, we need an adequate model to represent the SST. Unfortunately, some available SST global models do not work properly in shallow waters, especially close to the coast. If we do not have proper local SST models, we cannot obtain an accurate altimetric geoid in this kind of area because we cannot separate the mean oceanic signal from the result.

On the other hand, gravimetric data is more accurate and easier to obtain in shallow waters. As a matter of fact, it can be as accurate as data obtained on land. Consequently, it is better to compute a geoid from gravity data, without using altimetry. We will use the altimetry data, combined with gravimetric results, to obtain local models for the SST anywhere that no proper model is available. We will also see that in our test area the SST is correlated with the depths.

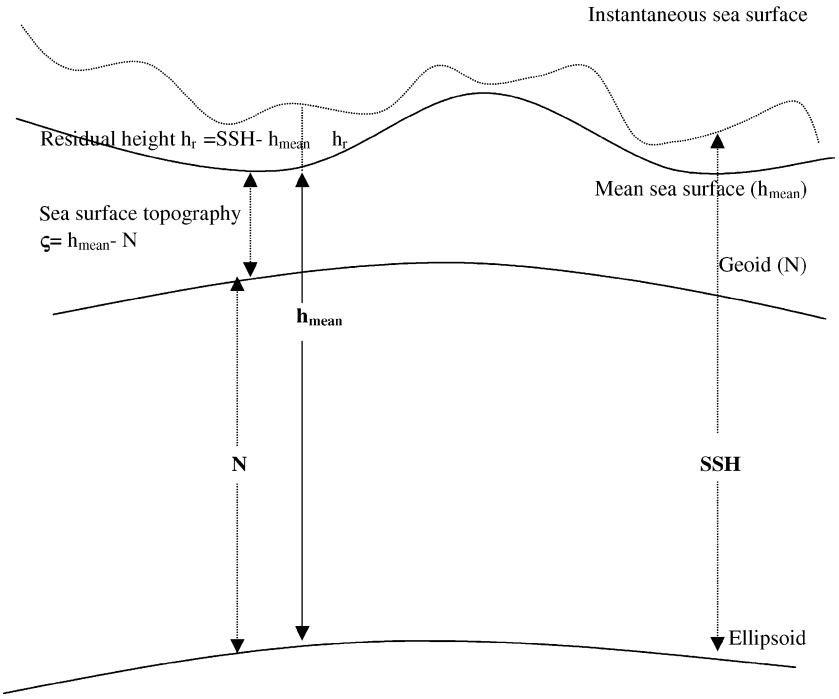

Figure 1. Involved surfaces.

2 GRAVIMETRIC GEOID

We built up a gravimetric geoid in the area bounded by: $38°5 < \phi < 41°5, 355° < \lambda < 2°$. The marine part belongs to the Mediterranean Sea. The data used was 9013 free air gravity anomalies from several sources: *Instituto de Astronomía y Geodesia,* IAG, *Instituto Geográfico Nacional Español,* IGNE and NIMA. Fig. 2 displays the geographical distribution of data throughout a half-degree area extending from prediction one in all directions. This data was validated and is referred to the same Geodetic Reference System, GRS80.

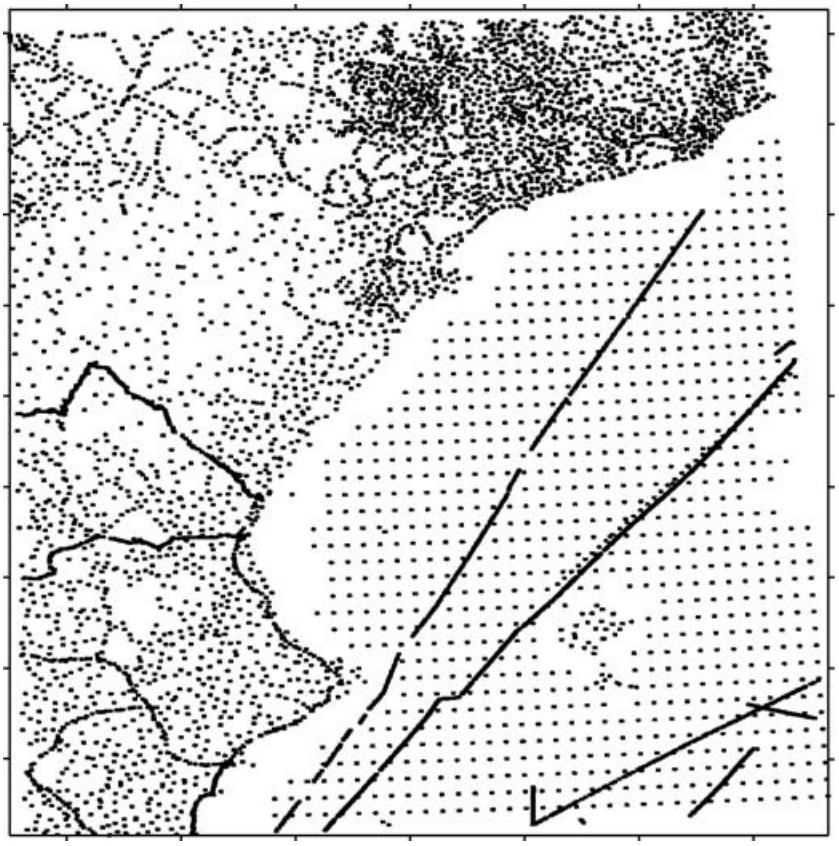

Figure 2. Distribution of available Δg.

The data was validated using the least-square collocation, LSC procedure with the classical remove-restore technique. Accordingly, the free air gravity anomalies are split into three components:

$$\Delta g = \Delta g_{\mathrm{MOD}} + \Delta g_{\mathrm{RTM}} + \Delta g_{\mathrm{RES}} \quad (1)$$

Δg_{MOD} represents the long wavelength part of the gravity field and was computed from the set of coefficients of the geopotential model OSU91A (Rapp *et al.* 1991) complete to degree and order 360. Later we found that the differences in the area between this model and the most recent EGM96 (Lemoine *et al.* 1997) are negligible. Δg_{RTM} is the topography effect or contribution of high frequencies to the gravity field, which was determined taking into account the deviations of real topography from a mean topography (residual terrain model) (Fosberg 1984). The corrections were made by using prism integration. The digital terrain models used were the MDT200 of the Spanish IGN (García Asensio *et al.* 1992), with a resolution of 200 m $\times$ 200 m, and ETOPO5 from NGDC (1988) for filling the gaps. A coarse model (with resolution of 1 km $\times$ 1 km) and a reference model (with resolution of 42 km in longitude and 56 km in latitude) were then generated by applying an average filter on them. The calculation radii used around the point were 15 km for the inner zone and 100 km for the outer zone. Δg_{RES} is the residual part of the signal.

Details about the LSC method and the complete formulation can be found in a wide selection of literature (Moritz 1980; Tscherning 1981). We only stress the fact that it can be used to estimate any gravity field-related quantity using:

$$S_{\mathrm{e}} = C_{\mathrm{P}}^{\mathrm{T}}(C + D)^{-1} S_{\mathrm{d}} \quad (2)$$

where S_{e} and S_{d} are the signals to predict and data respectively. In this case, S_{d} are always residual free air anomalies while S_{e} also represents reduced free air anomalies in the validation application and reduced geoid undulations in the other case. C_{P} is the covariance between both, C is the covariance of data and D the diagonal variance-covariance matrix of the data noise.

We selected samples of residual free air anomalies, distributed as homogeneously as possible to avoid prediction biases caused by an irregular distribution. These were used to generate empirical covariance functions. To take into account the different land and sea gravity field characteristics, we built up the covariances independently. We modeled the degree variances derived from the empirical covariance functions using an analytical model for the covariance (Tscherning & Rapp 1974), then used them to predict residual free air anomalies with the least-square collocation method for data not included in the samples. We rejected any points where large differences (10 mGals on land and 15 mGals on sea) were repeatedly found between data and predicted value and in doing so confirmed the compatibility of the different data sources. The accuracy of the data was then established with these values.

Table 1 shows the statistics of the validated free air gravity anomalies after each reduction, and the level lines of Δg_{RES} contoured with 10 mGals are displayed in Fig. 3.

The geoidal heights were also split into three parts in a similar way to the one shown in (1), as follows:

Table 1. Free air anomaly statistics.

	Mean (mGal)	S. deviation (mGal)	Range (mGal)
Δg	8.76	22.32	198.47
$\Delta g - \Delta g_{\mathrm{MOD}}$	−2.15	17.89	192.55
$\Delta g - \Delta g_{\mathrm{MOD}} - \Delta g_{\mathrm{RTM}}$	1.02	11.97	81.47

Table 2. Gravimetric geoid (N_{GRA}) statistics.

	Mean (m)	S. deviation (m)	Minimum (m)	Maximum (m)
1369 points	49.986	0.92	47.73	52.15

$$N_{\mathrm{GRA}} = N_{\mathrm{MOD}} + N_{\mathrm{RTM}} + N_{\mathrm{COL}} \quad (3)$$

The validated residual free air anomalies are used in formula 2 to obtain the residual geoid N_{COL}. N_{MOD} and N_{RTM} are the contributions of geopotential model and residual topography respectively, that are later restored to the geoid results obtained by collocation. Once again, the model of covariance function used was selected from (Tscherning & Rapp 1974). This time we used an empirical covariance function generated from marine and land data together to avoid coastal edge effects. Only minor discrepancies arise between using them separately or together. In the marine part of the area, which we will use afterwards, the corresponding differences have a mean value of −1 cm and standard deviation of 5.5 cm (Rodriguez 1999).

The geoid predictions were made over a grid of five minutes interval in both (latitude and longitude) directions. Contributions of geopotential model and topography are added back to the LSC estimations after (3). The result is a fairly smooth surface, especially in the marine part of the area. The isolines of this geoid are depicted in Fig. 4 and the statistics are shown in Table 2.

The covariance computations and LSC method were performed with the GRAVSOFT software package (Tscherning *et al.* 1992).

The collocation procedure lets us estimate the internal geoid accuracy. The estimated mean precision was 0.95 cm with a standard deviation of 25.5 cm. The highest error values were obtained on land, in an area associated to topographic features. This gravimetric geoid has been compared with other geoids in the area (Sevilla *et al.* 1992; Sevilla 1995). For instance, it has been compared with the geoid of the Iberian Peninsula, computed by application of Fast Fourier Transform. The geopotential model used was OSU91A and the topography effect was computed by using the Helmert second condensation reduction with a digital terrain model of resolution 1000 m $\times$ 1000 m. This Iberian geoid was controlled by GPS points, with an estimated accuracy of 1 ppm, that means, at 1 km distance, the difference between the variations of GPS heights and gravimetric geoid is 1 mm. All the compared results match well, and only differ in terms of centimeters. Once again, the biggest differences are located in mountainous areas and also in the south of Ibiza Island. In the first case, the discrepancies may be due to the different treatment of the topographic masses.

3 ALTIMETRIC DATA

We computed a local mean sea surface over the Western Mediterranean Sea, using CORSSH (corrected sea surfaces heights) data from ERS-1 generated by the CLS Space Oceanography Division (Toulouse, France) and distributed by AVISO/Altimetry CD-Roms. Beforehand the CORSSH data was fitted to TOPEX, therefore the precision should be similar to the TOPEX, accurate to 2 cm (Le Traon *et al.* 1995). We chose data from ERS-1 instead of TOPEX data directly because the TOPEX has a lower cross-track spatial distribution and hence is not suitable for conducting a study of such a small area. Specifically, the cross track spacing of the ERS data used is about one quarter of TOPEX data for this latitude.

The data consists of corrected sea surface heights, which were corrected during the preprocessing stage for geophysical effects

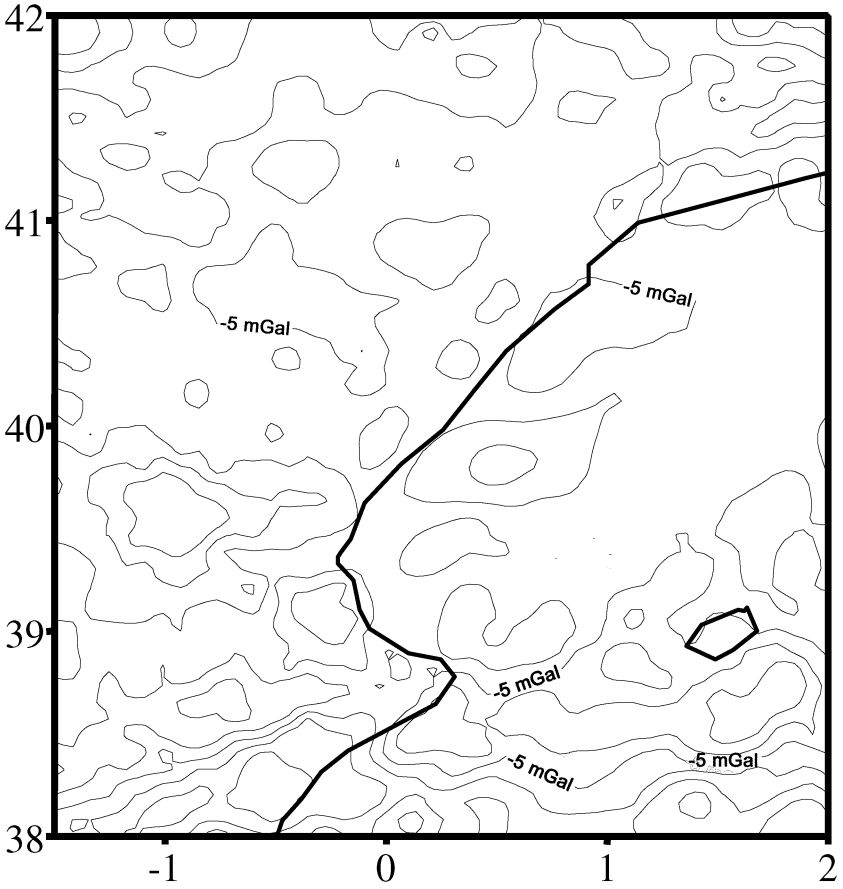

Figure 3. $\Delta g_{\rm res}$ contoured at 10 mGals interval.

(dry and wet tropospheric delay, inverse barometric effect and ionospheric delay), sea state bias, and tidal effects in a pre-processing stage. Ocean and loading tide effects were corrected using the CSR3.0 model with an estimated precision of 2–3 cm for depths above 200 m (Eanes & Bettadpur 1994) and the solid earth tide was computed with the Cartwright and Tayler model (AVISO/Altimetry 1996).

The data covers a period of approximately fifteen months of the second multidisciplinary phase (phase G), with repeat period of 35 days.

The gravimetric geoid covers a marine area too small to implement any crossover or so, adjustment of satellite data, so we selected measurements from a wider area ($35^\circ < \phi < 45^\circ, 345^\circ 5 < \lambda < 8^\circ 25$, except data from the Cantabrian Sea). The total number of data items is 218828. Fig. 5 displays the spatial distribution of data from a repeat cycle.

We edited the data to detect and remove some remaining incorrect data. We obtained residual heights $h_{\rm r}$ by subtracting the contribution of a global mean sea surface model MSS, namely the OSU95MSS (Yi 1995) from the corrected heights CORSSH.

$$h_{\rm r} = \text{CORSSH} - \text{MSS} \tag{4}$$

The residuals were used to detect incorrect data. Anyway, we did not expect gross errors since they were fitted to TOPEX. The following criteria were adopted:

(1) The measurements should not differ very much from the mean sea surface since the dynamic part does not exceed two meters (Arabelos & Tziavos 1996). Even this quantity is too big for an almost closed basin such as this. Therefore we rejected data where the residual height value $h_{\rm r}$ numerically exceeded 50 cm (more than the mean value). We only found 4 points that met this criterion, which are not located in any apparent pattern.

(2) We suppose that the corrected heights reproduce a fairly smooth surface. We looked for data with $\Delta\text{CORSSH}/\Delta t > 0.4$ m s^{-1} ($\sim 3\sigma$), where Δt is the time interval, between consecutive points. That means points where the observed surface is rough and there are big changes between successive measurements. We include Δt to observe the possibility of data interruptions. The chosen limit is quite small because we take into account that it is an almost closed sea, so it should stay quite calm. We found 11 randomly-distributed points. If the data was always distributed in the same location, it could not be a question of errors but true tilts, due to the correlation between sea surface and bathymetry as it has been seen in previous applications (Basu *et al.* 1990; Rodriguez *et al.* 1999).

(3) We looked for points with $\Delta(\text{COSSH} - \text{MSS})/\Delta t = \Delta h_{\rm r}/\Delta t > 0.4$ m s^{-1} (~half-range variation). If the region has a steep bathymetry, this criterion should be more suitable than the last one because the MSS also contains features caused by sea mounts. Hence this method finds points where the measurements display roughness that does not appear in the model. This criterion was used to select 24 points, with random geographical distribution.

A graphic validation was also performed and collinear track profiles were represented. Two samples are shown in Fig. 6. They clearly share very similar features in every analysed cycle but there is a bias between them. The mean separation between collinear tracks

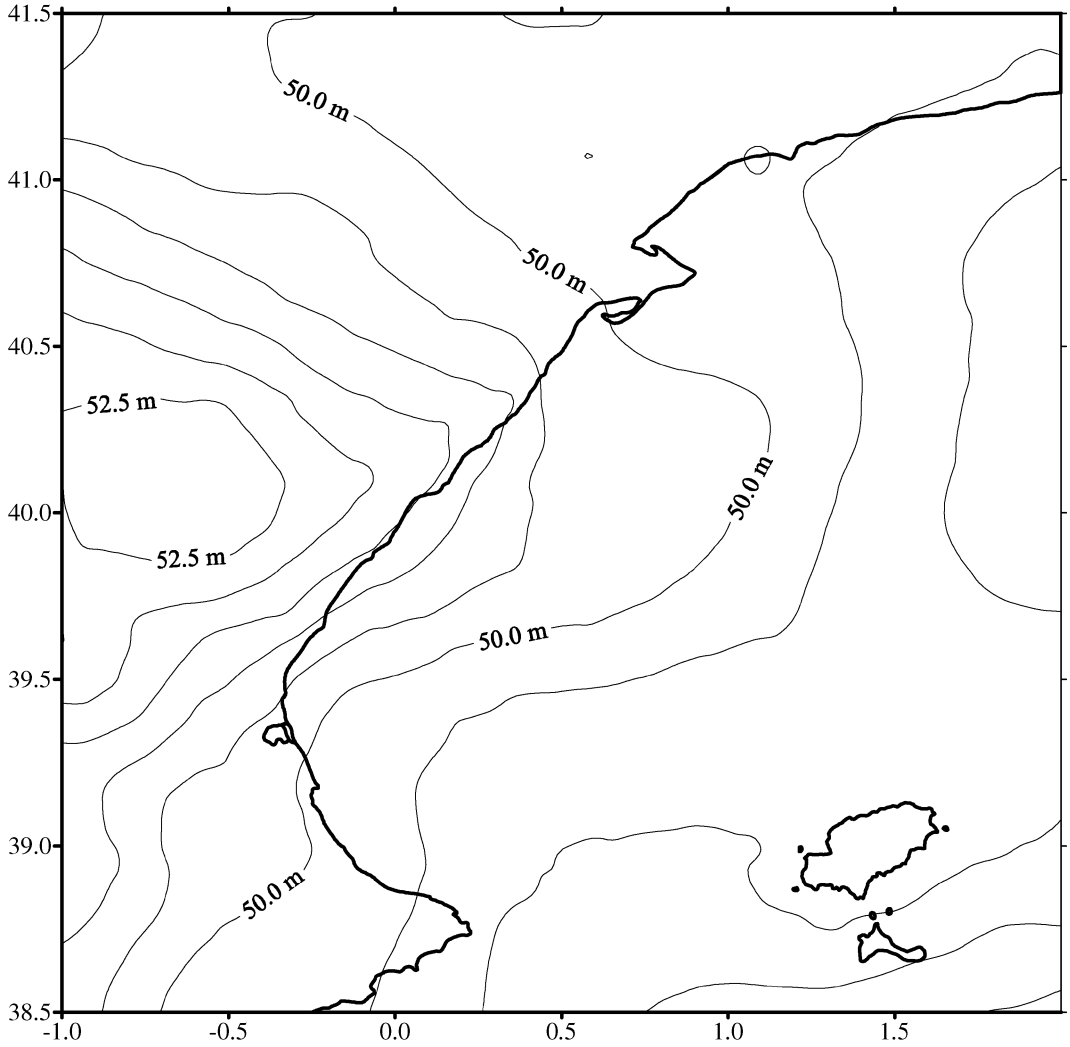

Figure 4. Gravimetric geoid (N_{GRA}). Contour interval: 0.5 m.

is around 30–34 cm, and sometimes up to 50 cm. We did not find any cycle or points displaying very different behaviour to the other collinear tracks, so no gross errors were detected.

Next, we wanted to see if the measurements changed near the coast and should be removed. To do so, we compared the three following surfaces: the corrected heights provided by the satellite, CORSSH, a gravimetric geoid developed in the context of the GEOMED (GEOid in the MEDiterranean) project, N'_{gra} (Sevilla *et al.* 1992) and the geoid model EGM96, or geoidal height above the described reference ellipsoid provided by the geopotential model to order and degree 360, N'_{mod}. The two last quantities were obtained by interpolation over the subsatellite points. This comparison was conducted graphically track by track. Some examples are shown in Fig. 7. Evidently, the three surfaces involved are not directly comparable, but they are good for validation purposes. The geoid surface is not the same as the altimetric surface. As it was exposed in the introduction, both differ in the SST plus errors in the two surfaces. Moreover, the geoid model only represents the long-mean wavelength part of N, while the gravimetric geoid also includes higher frequencies. Since the geoid has a long wavelength, the geopotential model provides its major contribution. Therefore the residual geoidal heights, N'_{gra}–N'_{mod}, should be small. We do not expect the three compared quantities to match, but nor do we expect major discrepancies between them, so large differences may point to erroneous data.

We expected continuity of the geoidal solutions near coast. We tried to analyse if all the altimetric data was correct or if we had to remove the data closest to the coast. There are clearly no major differences between the three profiles, even at the points nearest the coast. The comparison was performed by using one of the satellite passes as CORSSH, instead of the mean track. Since the previous phase demonstrated that the different colinear tracks do not differ greatly significantly, we did not repeat the comparison with every pass for the same ground track. The statistics of such differences are shown in Table 3:

$$\zeta_g = \text{CORSSH} - N'_{gra}$$
$$\zeta_m = \text{CORSSH} - N'_{mod} \quad (5)$$

Table 3. Statistics of the differences between the compared values of ς from different geoid solutions.

	Mean (m)	S. deviation (m)	Minimum (m)	Maximum (m)
ζ_g	0.417	0.312	−0.39	1.44
ζ_m	−0.251	0.22	−0.87	0.52

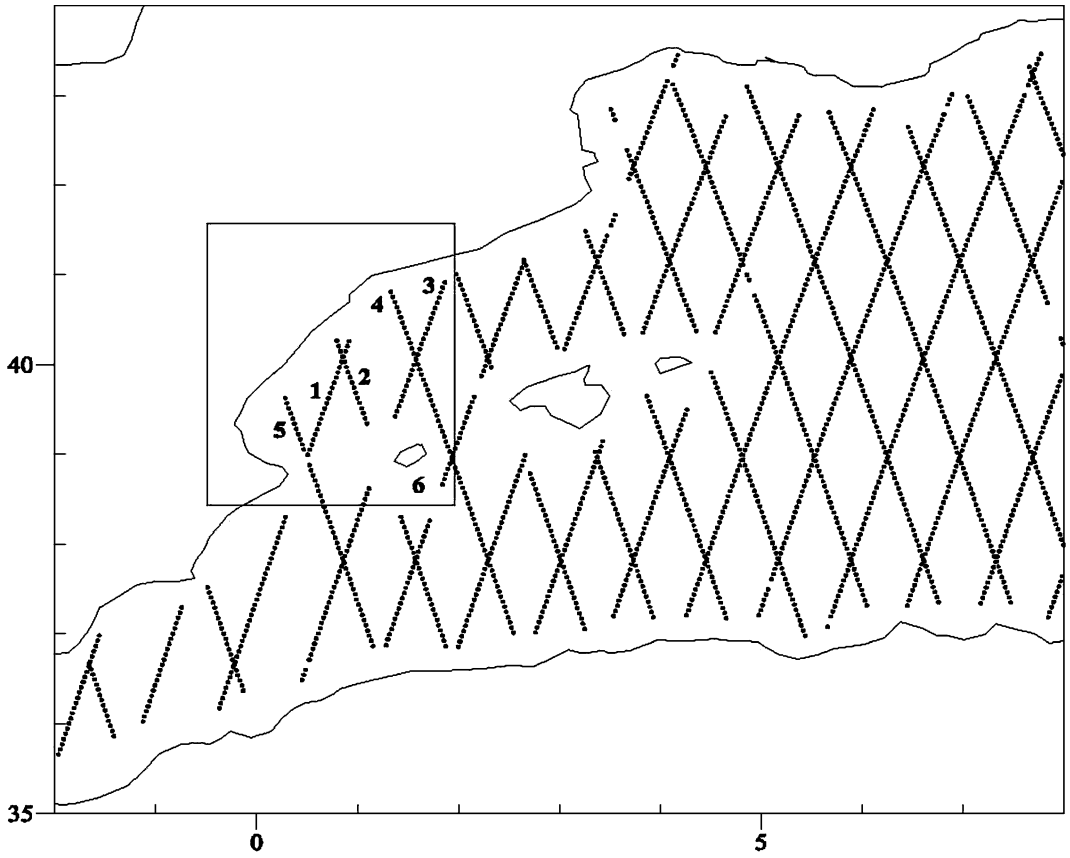

Figure 5. Spatial distribution of altimeter measurement over a repeat cycle. The square points at the area covered by the gravimetric geoid.

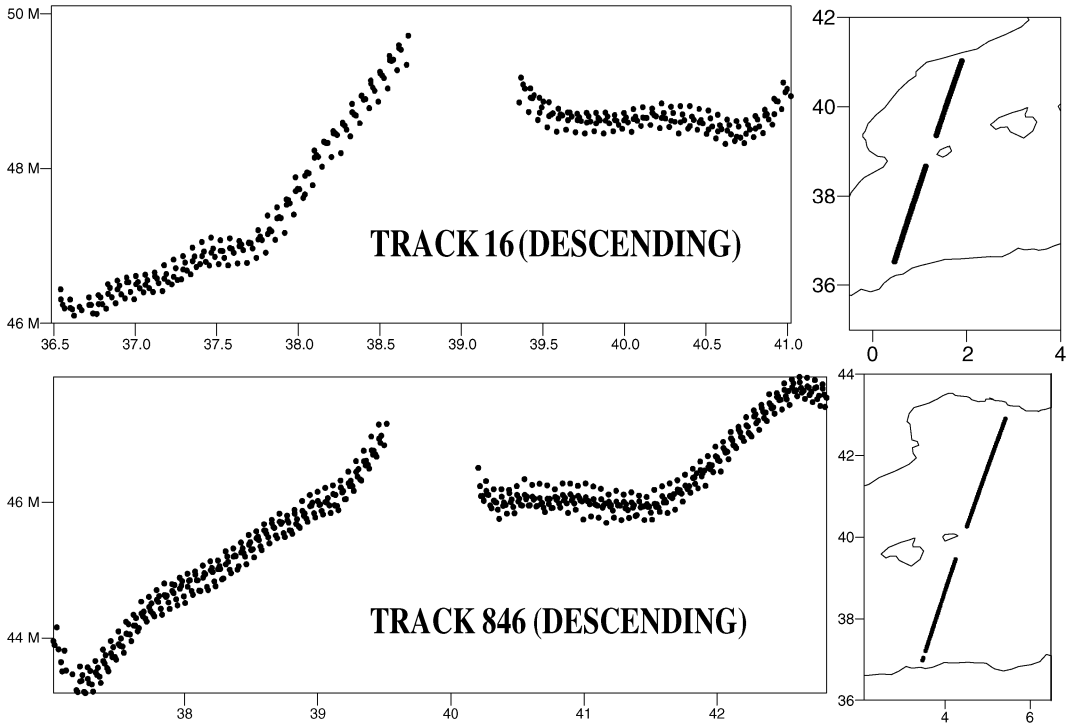

Figure 6. Two examples of repeated track.

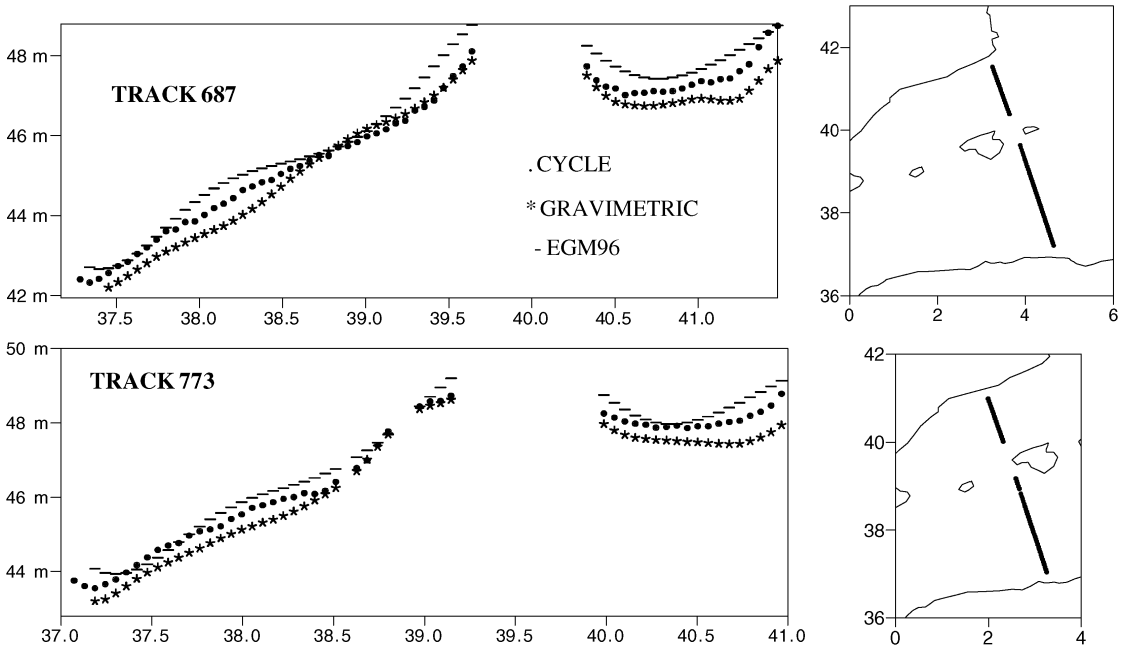

Figure 7. Two examples of the three surfaces comparison: N_{GRA}, N_{res} and CORSSH.

In both cases, the standard deviations are small and very similar each other. So, even if it is lower for the EGM96 geoid model, we cannot conclude very much about. In the test area, the measured sea surface is above the gravimetric geoid and bellow the model.

However, there are seasonal changes in the sea level. In the Northern Hemisphere the lowest levels occur in winter and spring (Tapley *et al.* 1994; Knudsen 1994). In a closed basin like this, such seasonal changes are bigger. There is less water than in an open ocean and the depths are smaller. Therefore any temperature and pressure changes have a bigger impact on a major proportion of water. The most heavily influenced part is the area of Algerian Currents, which occur due to the different density of the Atlantic and Mediterranean waters. The waters from the Atlantic flow from the Alboran basin to the west along the North African Coast. Most of the current originates in longitudes of 1–2 degrees. The generated adjacent currents are cyclonic and anticyclonic. The formers disappear fast, but the latter can change and move away from the main current. This sort of current is very persistent (cycles of six months have been observed) and is large in diameter (100 km). They move to the north and then lose energy and disappear slowly (Millot 1985). Moreover, the rest of this variation is caused by the imbalance between the incoming and outgoing flows at the Straits of Gibraltar, very close to the area in question.

Therefore we must take full years to average out most of this variability. Otherwise the resulting surface may contain biases depending on the majority of residuals of one or other sign. To see how suitable this selection was, we separated the data for the different seasons. Table 4 shows the variation of the residual heights during the year. As expected, they are mostly positive during the summer and fall. This trend changes during winter and spring. Therefore we will not use the data for all the fifteen months but only for one year.

4 LOCAL MEAN SEA SURFACE

The collinear tracks of ERS-1 were stacked to produce mean tracks. Averaging the heights along repeat profiles allowed us to remove some of the time-varying contributions. To do so, we selected data covering a year; that means 10 or 11 passes, depending on the ground track. This let us average out the seasonal variations.

The values were interpolated on a time grid defined by the best track in terms of the highest number of measurements. Residual heights were used instead of the full CORSHH to avoid MSS interpolation errors. The arc with the highest number of measurements was used as a reference and the orbit error was sinusoidal and therefore can be represented by any long wavelength function over a short arc length. To reduce the effects of such an error, the tracks were merged in a free adjustment using 1c/rev cosine and sine.

The stacking procedure let us reduce the number of data significantly, in this case to 1796 observations. Moreover, this process itself greatly reduces the effects of orbit errors and long wavelength variability (Arabelos & Tziavos 1996). Since the chosen interval is one year, the seasonal changes described before are averaged out, although the changes of longer periods remain, as does the geographically correlated orbit error.

The selected area is small and the irregular shapes of the coast and several islands interrupt the tracks, meaning that crossover adjustment could not be used. The rank deficiency of this adjustment is supposed to be p^2 with p, number of parameters and it is best to remove it by applying a low weight hybrid norm criterion. Therefore we tried to minimize the crossover differences and the discrepancies with a p^2 parameter surface. However, the rank deficiency is just p^2 in local applications only if there are more observations than parameters in the adjustment. This is not our case, so the

Table 4. Seasonal variation of h_r.

Season	Mean (cm)	S.D. (cm)	Min (cm)	Max (cm)	Range (cm)
Spring	−8	10	−44.3	37.4	81.7
Summer	2	9	−29.9	35.6	65.5
Fall	3	11	−48.6	41.1	89.7
Winter	−5	12	−49.7	32.3	82

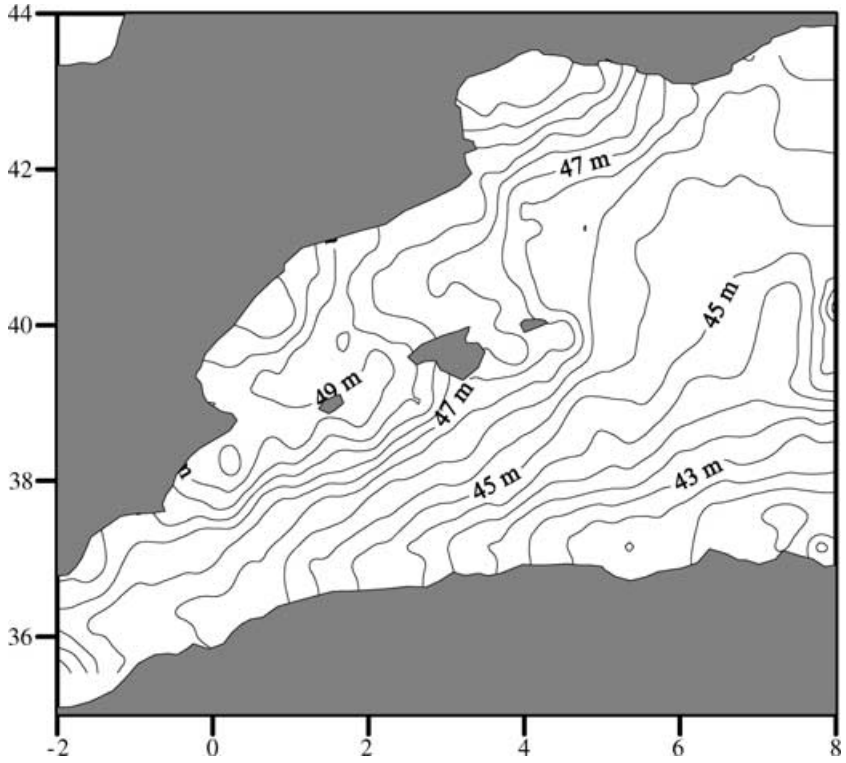

Figure 8. Level lines of the averaged altimetric surface (h_{mean}).

procedure could cause more errors. In the area we found 41 crossover points between ascending and descending passes from a total or intersecting 29 passes (meaning 54 parameters). Therefore the fitted mean sea surface estimation (h_{mean}) was the result of re-adding the OSU95MSS model (MSS) to the time stacked residual heights, (h_{m}) and we reject the crossover solutions.

$$h_{\text{mean}} = h_{\text{m}} + \text{MSS} \tag{6}$$

Fig. 8 displays the resulting surface, created by computing a grid with $\Delta\varphi$ and $\Delta\lambda$ equal to $0^{\circ}05$ with the commercial graphical software SURFER©, which permits several gridding methods. In this case, we chose the weighted average interpolator. The contour lines on the figure are placed at 50 cm intervals. Table 5 summarizes the result statistics. The mean value of h_{r} remains the same after the collinear adjustment, while the extreme values, and consequently the standard deviation, decrease significantly.

5 SEA SURFACE TOPOGRAPHY

The remaining part of the subtraction of the gravimetric geoid from the local mean sea surface from last section, contains the SST and the errors in both surfaces. The mean sea surface was generated from data covering one year and so does not include the seasonal changes. This is the main part of the ocean variation. In this study the differences are interpreted as the stationary SST, ς_{o}, plus the errors in the surfaces used, neglecting the mean sea surface variability ς_{r} because of its small value compared to ς_{o} (Heck & Rummel 1989).

Altimetric data was fitted to TOPEX, so it is assumed to be quite accurate. Then, the remaining errors are due to the shortest wavelength part of the geoid (and its errors). Because of the low value of this part of geoid, our results are a rough approach to the SST that we call ζ_1.

$$\zeta_1 = h_{\text{mean}} - N_{\text{GRA}} \tag{7}$$

As we have N_{GRA} over a regular grid, the corresponding values over the subsatellite points were interpolated using a spline prediction in a window of size 8×8 points around the point in question, in order to minimize the interpolating errors.

The differences are displayed in Figs 9 and 10. Table 6 gives the statistics of the two compared surfaces and their differences in the common part of the area. The order of magnitude is physically reasonable, because they can measure up to two meters (in open seas), although they tend to measure around 50 cm.

The stationary SST is mainly due to the dynamic balance between wind stress, pressure gradient and Coriolis force. The density difference between communicated basins also contributes. In shallow

Table 5. Results of the collinear analysis.

	Mean (m)	S.D. (m)	Min (m)	Max (m)	Range (m)
Residuals before applying collinear adjustment, h_{r}	−0.03	0.11	−0.53	0.39	0.92
Residuals after applying collinear adjustment, h_{m}	−0.031	0.045	−0.25	0.17	0.43
Averaged mean sea surface, h_{mean}	45.91	1.87	41.38	50.3	8.92

Table 6. Surface statistics in the common area.

(123 points)	Mean (m)	S. deviation (cm)	Min (m)	Max (m)
Gravimetric Geoid (N_{GRA})	49.33	48	48.3	50.2
Mean sea surface (h_{mean})	49.13	57.2	48.28	50.3
Differences (ζ_1)	−0.173	39.2	−0.78	0.96

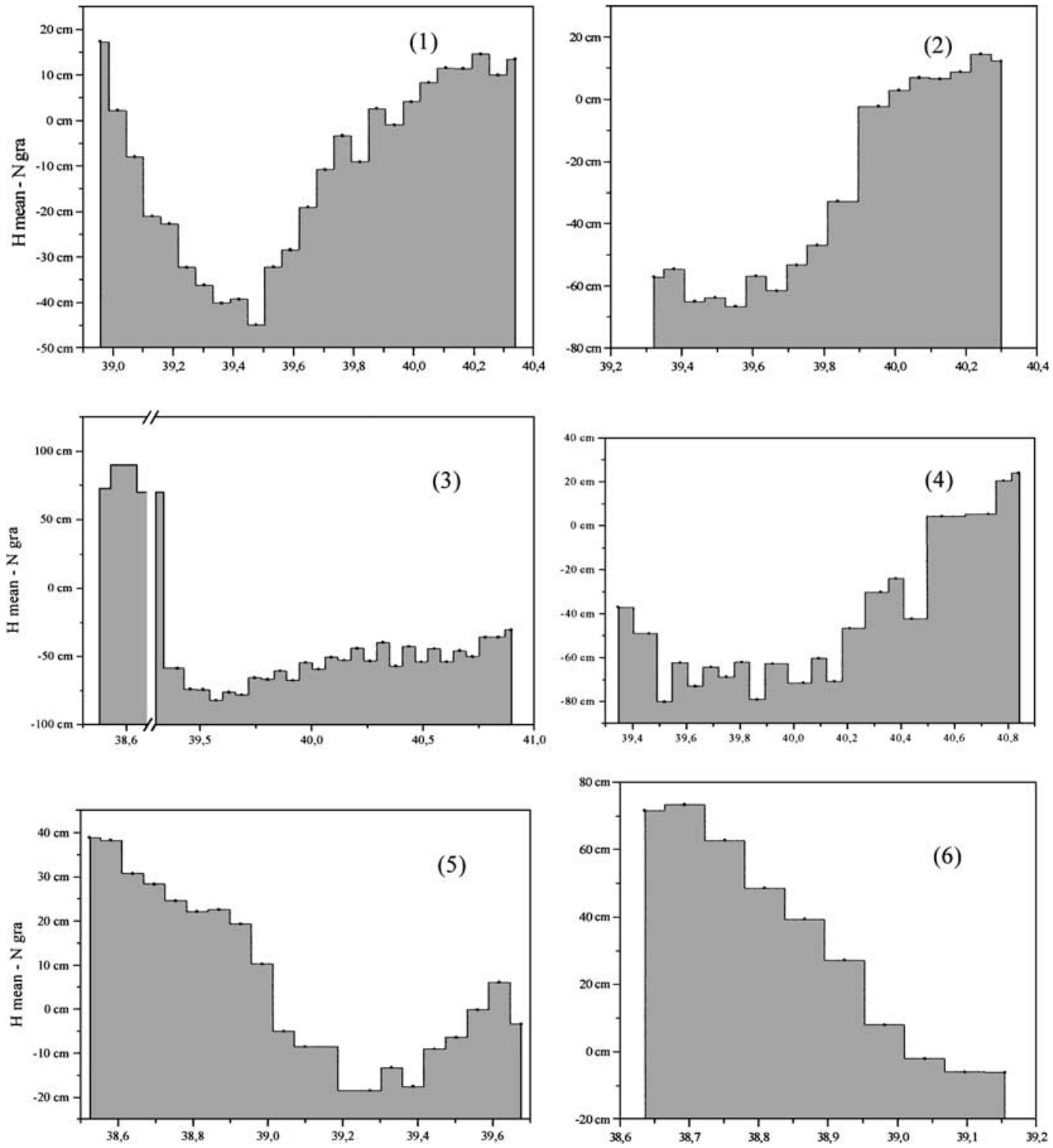

Figure 9. Differences between surfaces depicted track by track over the ones included in the area (see also Fig. 5).

waters and close to coastal lines, there are more complex processes and the SST is modified by local conditions (Hipkin 2000). As a result, the global models describing the SST, especially those from spherical harmonic expansions, do not work well in shallow waters or in depths above 1500–2000 m. Indeed, we have analysed the surface reproduced by two different global SST models in the area: OSU91A completed to degree and order 10, (Rapp *et al.* 1991) and EGM96, to degree and order 20 (Lemoine *et al.* 1997). Fig. 11 displays the isolines of the two models, which do not resemble the ones in Fig. 10 (our first SST estimation). Yet they also differ from one to another. The lines follow a similar pattern, though the OSU91A isolines are flatter, but the assigned values are different. EGM96 has a smaller range of variation. In the northern part of the area, the two have very similar values, but the differences increase as the latitude decreases. In the central part of the area the discrepancy is around 10 cm (see the islands), increasing in the south to values in excess of 15 cm. These differences may be due to the different order considered in the computations.

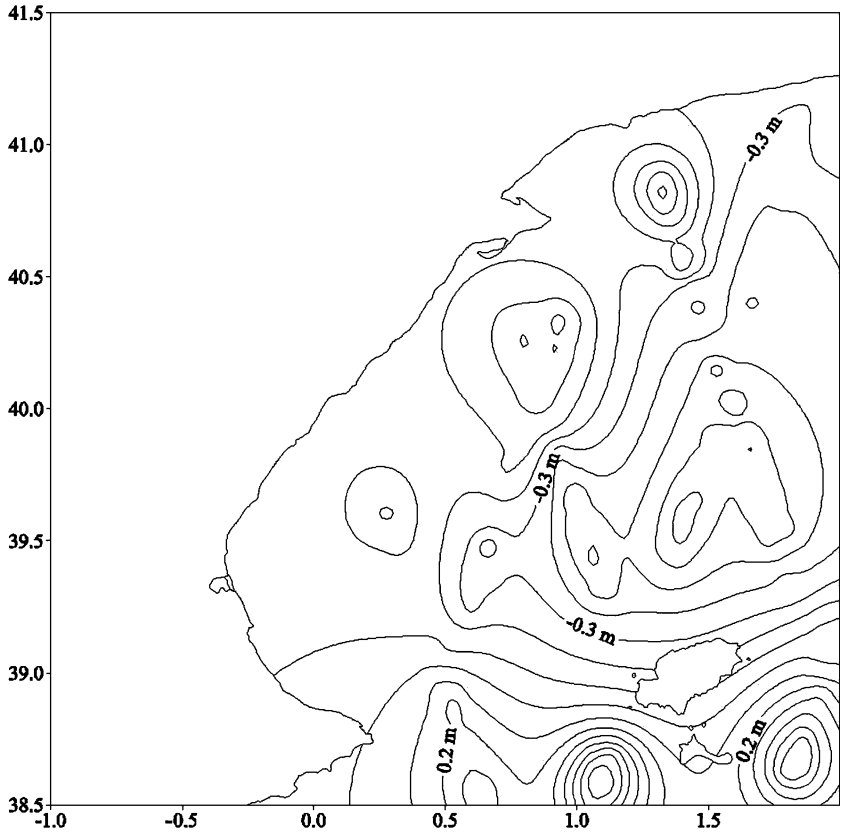

Figure 10. First estimation of the static SST (ζ_1) contoured at 10 cm interval.

6 BATHYMETRY IN THE AREA

We consider several bathymetric models in this area: the aforementioned ETOPO5, one obtained from Morelli's maps and the Terrain-Base from NGDC (Row *et al.* 1995). The three of them share fairly similar features in this region, as may be seen in Fig. 12.

Figs 9 and 12 clearly show that most of the tracks have similar features. Before we can say that there is a general correlation between the sea bottom bathymetry and the SST, we must make sure that this is not due to some of the surfaces used. We take into account that the model used to compute the topography contribution to the geoid has been one of them, so the geoid solution already includes the influence of the represented bathymetry.

The altimeter data is accurate, but the reductions applied to them involve using tidal models. These models are usually less accurate in shallow water areas, so one might wonder whether the observed correlation is due to depth-related errors in the altimetric surface. We can confirm that this correlation is not due to altimetric data reductions if we find currents in the region, because current flows are closely correlated to sea bottom topography and the SST is related to current velocity.

The area in question is quite complex from a dynamic point of view. It is very close to the area of propagation of the Algerian Currents, already described in Section 3. Due to the density gradient between Atlantic and Mediterranean waters, these currents constitute one of the major oceanographic features of the basin (Le Traon *et al.* 1997). It is also next to the Alboran Sea, where there is significant activity. Some surface speeds reach values of 1 m s^{-1}, giving rise to anticyclonic gyres (Beckers *et al.* 1997).

Yet this part is itself a region with important circulation. There is a zone of special circulation in the so-called Balearic Sea, or portion of water between the Balearic Islands and the Northeast coast of Spain.

The Atlantic waters enter the Sardinian Channel, although part of it does not enter the Eastern Basin through the Straits of Sicily. This part of the water does not circulate in a normal geostrophic pattern due to interaction with other currents. It goes on around the Tyrrhenian Sea, leaves through the Corsica Channel and joins the Corsica Current to form an important cyclonic gyre, the Northern Mediterranean Current (Lehucher *et al.* 1997) also known as Ligurian-Provençal-Catalan Current.

Dense water forms under the influence of evaporation and surface cooling in the Gulf of Lions shelf. Another factor is the propagation in this zone of some very cold and dry continental winds (e.g. Tramontana and Mistral), produced by the mixing and convection process (Astraldi & Gasparini 1992). There, the Atlantic water turns into Mediterranean water and becomes denser. The process occurs in the Western basin below 800 m. This is an important event that only happens in a few places such as some areas of the Artic and Antarctic and in the Red Sea. This formation drives a significant part of the Northern Mediterranean Current. The Current enters the area in question from the Gulf of Lions, continues south-west, contouring the Western part of the Gulf and the Catalan Coast, and goes back along the northern slope of the Balearics (Canals *et al.* 1997).

Temperature regimes and wind speed guide ocean dynamics. In this case, the inflow of surface Atlantic waters through the west Balearic passages may also change the main circulation path. The area in question includes part of the Balearic Islands. It is a very

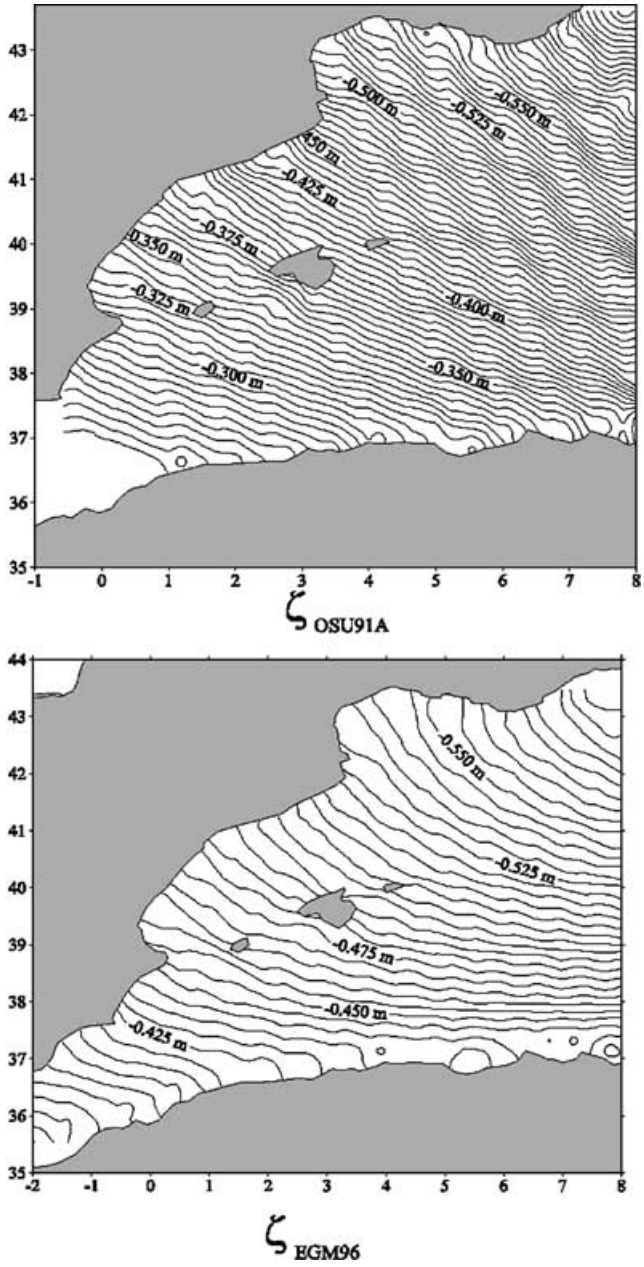

Figure 11. Global models of SST in the area. Contour interval, 0.5 cm.

complicated region because the islands act as a buffer, limiting the Alboran basin (interchange with Atlantic water) and Ligurian-Provençal basin (current).

The last oceanic feature observed in the area is that an anticyclonic gyre occupies most of the shelf on the Gulf of Valencia (from latitude 38°8 to 39°5) where continental waters run off and recirculate (Lehucher *et al.* 1997).

The conclusion drawn can be that, in this area of shallow water, ζ_o is closely correlated to bathymetry. Therefore it is natural to consider a better fit to the SST by using an increasing depth function. This could help us to separate the real SST part and the short wavelength part of the geoid and errors from ζ_1.

In particular, we tested several models. Their parameters were estimated by a least-square procedure taking the differences or ζ_1 values as observations. All of them were considered with the same weight. We started with a linear regression ($\zeta = A + Bh$) between the first estimation of SST, ζ_1, and the bathymetry, h. The results of the adjustment are displayed in Table 7, which shows that the error values of each parameter are quite small. The standard deviation of the adjustment is 0.23793. Fig. 13 shows the location of the points and the adjusted function.

Table 7. Results of the adjustment of a linear function: A + Bh.

Parameter	Estimated value	Error
A	0.30197 m	0.04051
B	0.000608258	0.000041326

Using parameters A and B of the adjustment and the Terrain-Base depths, we built an approximation to the SST with the model determined from the depths (ζ_a). The resulting surface is shown in Fig. 14 and it is clear that this result globally reproduces the same features as the ones displayed in Fig. 10. This occurs because, as expected, the function is an increasing one, as can seen from Table 7, where parameter B, the slope, is positive. The extreme values of depth and estimated SST occur at the same locations.

The linear fit is an easy way to find a first and quick mathematical model for the correlation. Using more complex, increasing function models does not improve matters at all. For instance, instead of linear regression, we can also fit the ζ_1 values to a two-degree polynomial: $\zeta = A + Bh + Ch^2$. In this case, as seen in Table 8, the B and C parameter errors are similar and thus rather uncertain. The standard deviation is 0.22075, very similar to the one obtained in the linear adjustment. We verified that this polynomial is also increasing to see if it displays the same features again. This occurs because its derivate, B + 2Ch is a positive value for each $h < 0$, like the ones in a marine region (2Ch > −B, $h < -B/2C$, bigger than zero). The data points and adjusted function are shown in Fig. 15. The surface that appears if this model (ζ_b) is used with the depths in the area is depicted in Fig. 16.

We also tried a polynomial fit of fourth degree. The results (ζ_c) are given in Table 9 and show that the errors are sometimes bigger than the estimated value itself. However, the standard deviation, 0.20559, is not bigger than in the last fit. Moreover the resulting function is not always an increasing function, as shown in Fig. 17.

Table 10 shows the statistics of the three sea surface topographies estimated by the proposed models. All of them are quite similar to the one shown in Table 6. Table 11 lists the statistics of residuals of the computed surfaces. The lowest average is reached when the

Table 8. Results of a second degree polynomial $A + Bh + Ch^2$.

Parameter	Estimated value	Error
A	0.12294 m	0.05377
B	−0.000225341	0.000176878
C	−0.000000527596	0.0000000109394

Table 9. Results of a fourth degree polynomial $A + Bh + Ch^2 + Dh^3 + Eh^4$.

Parameter	Estimated value	Error
A	−0.08679 m	0.10006
B	−0.00201	0.000988788
C	−0.00000343727	0.00000253972
D	$-1.25168\ 10^{-9}$	$2.36025\ 10^{-9}$
E	$-8.85372\ 10^{-15}$	$7.24233\ 10^{-13}$

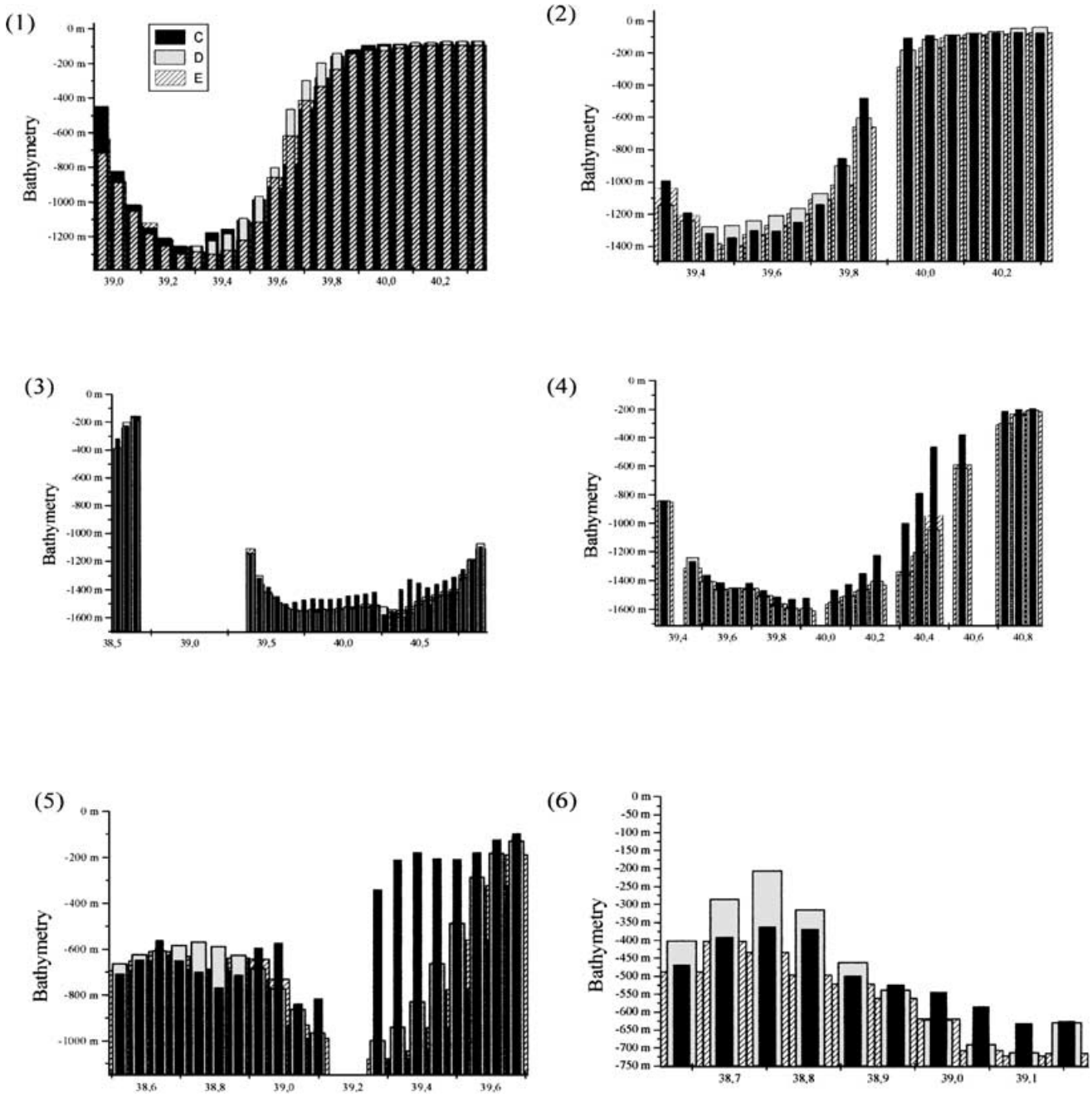

Figure 12. Local bathymetry track by track. C, means Terrain-Base, D, ETOPO5U and E, bathymetry from Morelli's map.

2-parameter model is used, but the differences are larger. The lowest standard deviation is obtained using the four parameter adjustment, and this could be regarded as being the most efficient, but there are certain drawbacks. First, this would only be a local conclusion that could not be extrapolated to other areas unless we tested it in them. Moreover, the errors of some of this model's parameters are larger than the parameters themselves. In all cases, the smaller depths display the most irregular patterns of behaviour. This fact

Table 10. Statistics of the three computed surfaces as functions of depth.

	Mean (cm)	S. deviation (cm)	Minimum (cm)	Maximum (cm)
ζ_a	−20.3764	31.5755	−65.7	26
ζ_b	−19.6577	32.9582	−83.4	14.7
ζ_c	−20.0081	34.2138	−62.6	25

Table 11. Statistics of their differences with ζ_1.

	Mean (cm)	S. deviation (cm)	Minimum (cm)	Maximum (cm)
$\zeta_1 - \zeta_a$	0.7195	23.8203	−42.5	76.9
$\zeta_1 - \zeta_b$	$8.13\ 10^{-4}$	21.8065	−51.8	78.8
$\zeta_1 - \zeta_c$	0.35122	20.1339	−63.5	73

may be due to errors in the tidal correction, which is not so accurate for depths above 200 m as described in Section 3.

These function models should be able to filter out the errors in the surface. Geoid errors should affect the short wavelength part, since the geopotential models are accurate enough to represent the low frequency part properly.

The functions can be improved by not only considering the depths but also the area sedimentary type. The Northeast margins including

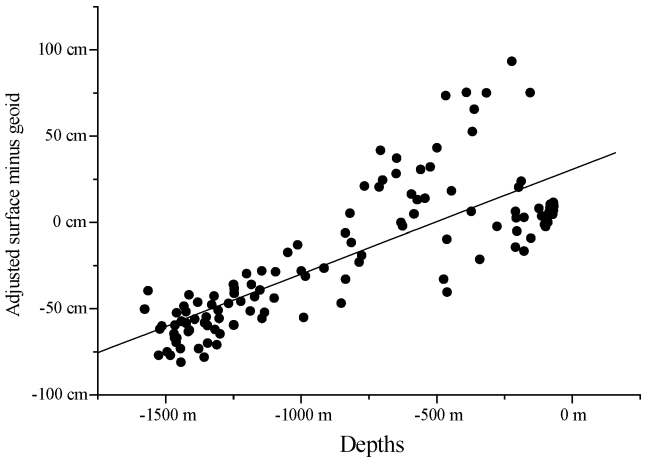

Figure 13. Linear fitting of the points.

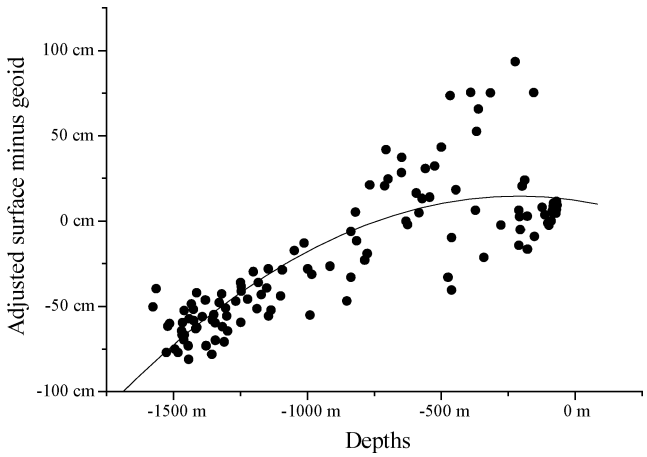

Figure 15. Polynomial fitting, degree 2.

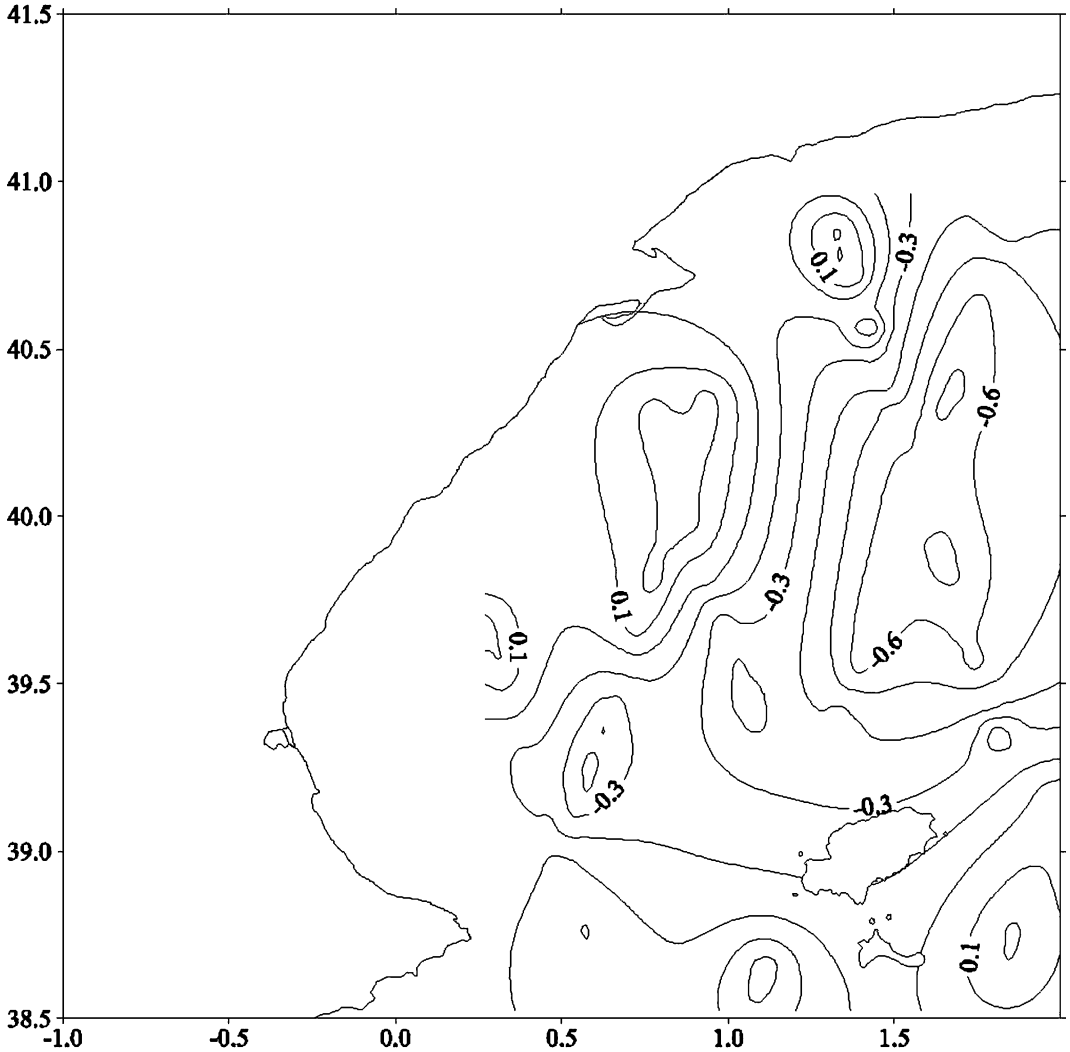

Figure 14. Linear SST local model contoured at 5 cm interval.

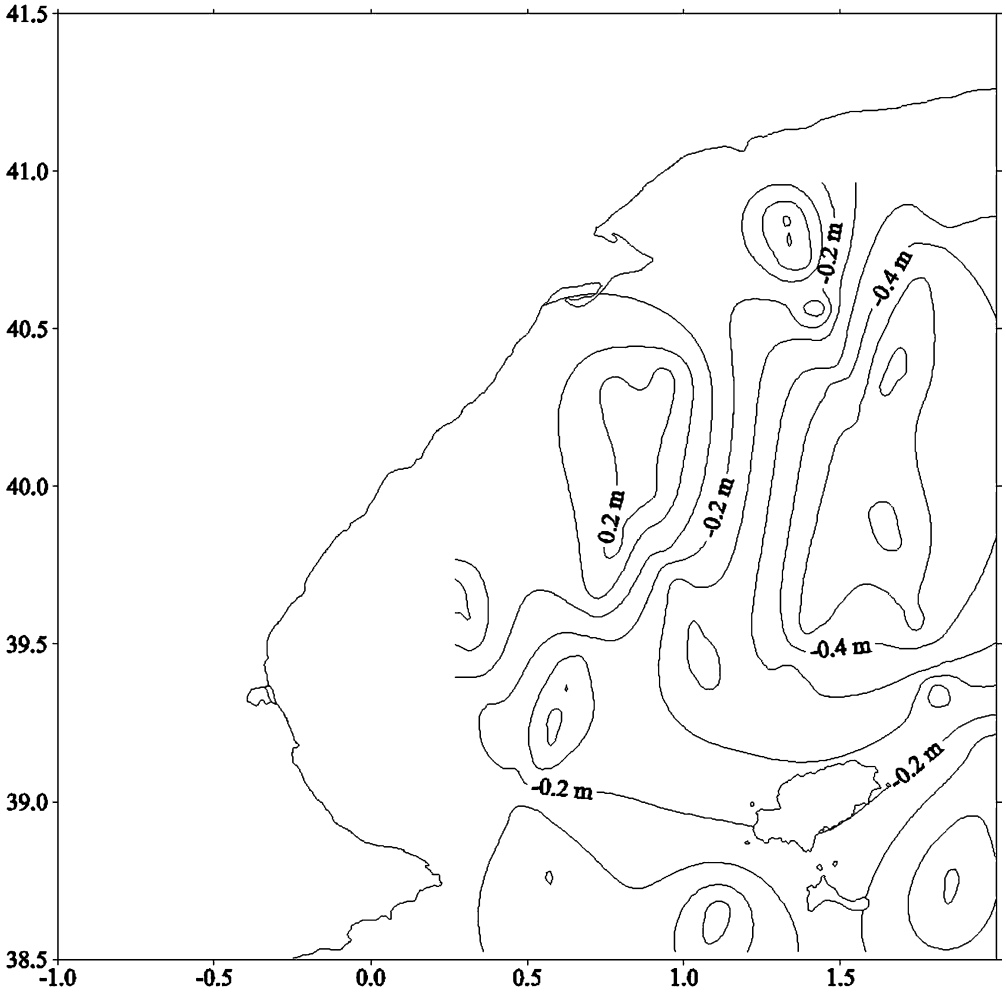

Figure 16. Second degree SST local model contoured at 5 cm interval.

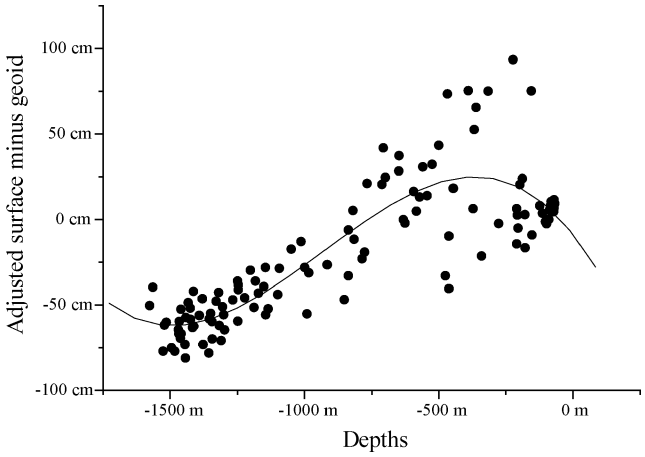

Figure 17. Polynomial fit of fourth degree.

the Ebro margins are terrigenous, while the Balearic margin is carbonated (Canals *et al.* 1997). This may affect the correlation.

7 CONCLUSIONS

Gravimetric and altimeter data was analysed to build-up a local geoid and a local mean sea surface for a region in the Western Mediterranean Sea.

The LSC procedure was used to validate free air gravity anomalies and estimate geoidal heights. Land data was included to avoid edge effects on the results. The collocation procedure allowed us to estimate the internal accuracy, but we also performed comparisons with other geoid results to assess the accuracy of the estimate.

The altimeter data was taken from fifteen months of the ERS-1 mission. This satellite was selected on account of its higher spatial resolution, which is more appropriate for a restricted area like this. In a previous stage, data was fitted to TOPEX to improve its accuracy. Using the data for one year, the residual heights referred to a global mean sea surface model (OSU95) were adjusted collinearly in order to remove as many as possible of the radial orbit errors and regular seasonal changes. By adding back the subtracted model we obtain a local mean sea surface for the region.

In a second stage, the computed geoid was compared to the derived local mean sea surface. The results constitute a rough approximation to the SST in the area, ζ_1. The surfaces used in this approximation also contain errors.

We can assume that altimeter data is as accurate as TOPEX data because of the pre-proccessing. Therefore the derived mean sea surface is chosen for reference purposes. However, this first SST solution contains the short wavelength part of the geoid, which has to be filtered out from the result.

An important similarity is observed between the features obtained by the SST estimation and the bathymetry in the area. After excluding that it is due to other factors, we can assess an approximation

to SST by using depth functions. Assuming this correlation, we can obtain a more accurate SST by removing from ζ_1, part of the remaining signal due to the geoid and other errors.

Future assignments include, first, contrasting these results in other basins in order to see their generality, and second, comparing the estimate of the SST obtained by bathymetry and models based on oceanographic studies and current flows that may reproduce local features better. The sedimentary part of the different parts of the basin will be also considered in the future to obtain a more realistic function model to describe the SST.

ACKNOWLEDGMENTS

This research has been mainly supported with funds from research project AMB99-1015-C02-01 of CICYT. The CORSSH products are supplied by the CLS Space Oceanography Division, Toulouse, France. The ERS products were generated as part of the proposal 'Joint analysis of ERS-1, ERS-2, and TOPEX/Poseidon altimetry data for oceanic circulation studies'. We also want to thank the reviewers for their comments and suggestions.

REFERENCES

Arabelos, D. & Tziavos, I.N., 1996. Combination of ERS-1 and TOPEX altimetry for precise geoid and gravity recovery in the Mediterranean Sea, *Geophys. J. Int.,* **125,** 285–302.

Astraldi, M. & Gasparini, G.P., 1992. The seasonal characteristics of the circulation in the North Mediterranean basin and their relationship with the atmospheric climatic conditions, *J. geophys. Res.,* **97,** 9531–9540.

AVISO/Altimetry, 1996. *Aviso User Handbook for Corrected Sea Surface Heights Altimeter Products,* 2nd edn, AVI-NT-011-311-CN.

Basu, S., Gairola, R.M. & Pandey, P.C., 1990. Collinear track analysis of Geosat Altimeter Data fort detecting seamounts in the Arabian Sea, *Marine Geodesy,* **14,** 121–135.

Beckers, J.M., Brasseur, P. & Nihoul, J.C.J., 1997. Circulation of the Western Mediterranean: from global to regional scales, *Deep Sea Research II*, *Vol. 44,* **3–4,** 531–549.

Canals, M. *et al.*, 1997. Transfer of matter and energy in European continental margins, in *Interdisciplinary research in the Mediterranean Sea,* pp. 31–68, ed. Lipiatou, E., A synthesis of scientific results from the Mediterranean targeted project (MTP) Phase T (1993–96). EUR. 17787 EN. ISSN:1018-5593.

Eanes, R.J. & Bettadpur, S.V., 1994. Ocean tides from two years of TOPEX/Poseidon altimetry, *EOS, Trans, AGU,* **75,** 61.

Fosberg, R., 1984. A study of terrain reductions, density anomalies and geophysical inversion methods in gravity field modelling, *Dept. of Geodetic Science and Surveying Report,* no. 355, OSU, Columbus, Ohio.

García Asensio, L., Lumbreras, J.J., Martín, G. & Heras, C., 1992. La Altimetría en el SIG del IGN. Modelos digitales de Terreno, *Nota Técnica de Geodesia,* NIG5. IGN. Madrid.

Heck, B. & Rummel, R., 1989. Strategies for solving the vertical datum problem using terrestrial and satellite geodetic data, in *Sea Surface Topography and the Geoid*. International Association of Geodesy Symposia, **104,** 116–128, Springer-Verlag.

Hipkin, R., 2000. Modelling the geoid and sea-surface topography in coastal areas, *Phys. Chem. Earth,* **25,** 9–16.

Knudsen, P., 1994. Global low harmonic degree models of the seasonal variability and residual ocean tides from T/P altimeter data, *J. geophys. Res.,* **99,** NC12, 24 643–24 655.

Lemoine, F. *et al.*, 1997. The development of the NASA/GSFC and DMA Joint Geopotential Model, *Iproc. Int. Symp. Gravity, Geiod and Marine Geodesy (GRACEOMAR). IAG Symposium Series,* Vol. 117, 461–469, eds Segawa, *et al.*, Springer-Verlag.

Lehucher, P.M., Astraldi, M., Millot, C., Beckers, J.M., Fonts, J., Chabert d'Hiéres, H., Crepon, N. & Tintoré, J., 1997. The hydrodynamics of the Western Mediterranean Sea, in *Interdisciplinary research in the Mediterranean Sea,* ed. Lipiatou, E., A synthesis of scientific results from the Mediterranean targeted project (MTP) Phase T (1993–96). EUR. 17787 EN. ISSN:1018-5593.

Le Traon, P.Y., Gaspar, P., Boyssel, F. & Makhmara, H., 1995. Using TOPEX/Poseidon data to enhance ERS-1 data, *J. Atm. Ocean Techn.,* **12,** 161–170. National Geophysical Data Centre, 1988. Digital relief of the surface of the Earth, *NOAA NGDC Data Announcement*. Boulder, Colorado.

Le Traon, P.Y., Ogor, F., Ayoub, N., Ducet, N. & Hernandez, F., 1997. Sea level variability from ERS-1, ERS-2 and TOPEX/Poseion, in *Proceedings of the Third ERS Symposium on Space at the Service of our Environment.* ESA SP. 414. Vol. III.

Millot, C., 1985. Some features at the Algerian Current, *Journal of Geophysical Research,* **90,** 7169–7176.

Moritz, H., 1980. *Advanced Physical Geodesy.* Helbert Wichmann Verlag, Karlsrure.

Rapp, R.H., Wang, Y.M. & Pavlis, N.K., 1991. The Ohio State 1991 geopotential and sea surface topography harmonic coefficient models, *Dept. of Geodes. Science Report,* **410,** OSU.

Rodríguez, 1999. Estudios sobre geoides terrestres y marinos, *PhD Thesis,* p. 319. Univ. Complutense de Madrid, Spain.

Rodríguez, G., Sevilla, M.J. & Toro, C., 1999. Validation criteria for ERS-1 altimetric datain the North Atlantic. Relation with problematic areas. Presented at XXIVth General Assembly of European Geophysical Society. The Hague.

Row, L.W., Hasting, D.A. & Dunvbav, P.K., 1995. Terrain Base Worldwide Digital Terrain Data. CD-Rom release 1.0. NOAA, NGDC, Boulder, Colorado.

Rummel, 1993. Lecture notes in Earth Sciences, **50,** 190–243, Springer-Verlag.

Sevilla. M.J., Rodríguez-Caderot, G. & Gil, A.J., 1992. A gravimetric geoid in the Mediterranean Sea, *Mare Nostrum, GEOMED Report,* **1,** 37–83.

Sevilla, M.J., 1995. A new gravimetric geoid in the Iberian Peninsula, *Bureau Gravimetrique International, BGI. Bulletin d'Information 77, International Geoid Service, IGeS Bulletin,* **4,** 163–180.

Tapley, B.D., Chambers, D.P., Shum, C.K., Eanes, R.J., Ries, J.C. & Stewart, R.H., 1994. Accuracy assessment of the large scale dynamic topography from TOPEX/Poseidon altimetry, *J. geophys. Res.,* **99,** 24 605–24 617.

Tscherning, C.C. & Rapp, R., 1974. Closed covariance expressions for gravity anomalies, geoid undulations and deflections of the vertical implied degree variance models, *Dept. of Geod. Science Report,* **208,** OSU.

Tscherning, C.C., 1981. Comparison of some methods for the detailed representation of the earth's gravity field, *Rev. Geophys. Space Phys.,* **19,** 213–221.

Tscherning, C.C., Fosberg, R. & Knudsen, P., 1992. The GRAVSOFT package for geoid determination. Presented at *Continued Workshop on the European Geoid.,* Prague. May.

Visser, P.N.A.M., Wakker, K.F. & Ambrosius, B.A.C., 1993. Dynamic Sea Surface Topography from GEOSAT Altimetry, *Marine Geodesy,* **16,** 215–239.

Wang, Y.M. & Rapp, R.H., 1994. Estimation of Dynamic Topography, Ocean Tides and Secular Changes from Altimeter Data, *Dept. of Geodes. Science Report,* **430,** OSU.

Yi, Y., 1995. Determination of gridded mean sea surface from TOPEX, ERS-1 and GEOSAT altimeter data, *Dept. of Geodes. Science Report,* **434,** OSU.